# Bend-tolerant fiber sensor based on BOTDR system*

**LI Yongqian[1,2,3], FAN Haijun[1,2,3]**, WANG Lei[1,2,3], ZHANG Lixin[1,2,3], and LIU Ting[1,2,3]**

*1. Department of Electronic and Communication Engineering, North China Electric Power University, Baoding 071003, China*

*2. Hebei Key Laboratory of Power Internet of Things Technology, North China Electric Power University, Baoding 071003, China*

*3. Baoding Key Laboratory of Optical Fiber Sensing and Optical Communication Technology, North China Electric Power University, Baoding 071003, China*

(Received 7 November 2021; Revised 28 January 2022)



A simple and inexpensive sensing structure, single mode fiber (SMF) alignment fusion to 62.5 μm stepped index-multimode fiber (SI-MMF), combined with Brillouin optical time domain reflectometry (BOTDR) system, is used as a distributed sensor in the field of structural safety and health monitoring (SSHM) of large infrastructures in terms of its prominent bending resistance. The bend loss principle and influencing factors of the fiber are analyzed, and the bending resistances of different fibers are discussed on the basis of theoretical and experimental comparisons. The bend-tolerant capacity and temperature sensing characteristics of the 5 km sensing structure are measured by using the self-developed frequency-shifted local heterodyne BOTDR system. The results show that the proposed sensing structure has excellent bend-tolerant capacity with a minimum bend radius and temperature measurement error of 1.25 mm and 0.69 °C, respectively, which indicates that the proposed sensing structure has huge potential in the field of SSHM of large infrastructures.

**Document code:** A **Article ID:** 1673-1905(2022)06-0343-6

**DOI** https://doi.org/10.1007/s11801-022-1172-0

In recent years, Brillouin optical time domain reflectometry (BOTDR) based on single mode fiber (SMF) has been widely studied in the field of structural safety and health monitoring (SSHM) of large infrastructures, such as bridges, tunnels, dams and large buildings[1-5]. BOTDR, a structurally simple operating system, uses the linear relationship between the spontaneous Brillouin scattering optical power or Brillouin frequency shift (*BFS*) and the changes of temperature and strain to realize the fully distributed sensing along the fiber. Several techniques have been developed to improve the performance of BOTDR sensing system, such as frequency shift-averaging[6], pulse coding[7-9], multi-wavelength[10], differential pulse pair[11] and broad-band laser[12], etc. However, in the practical SSHM, multiple bends will inevitably be introduced in the process of fiber laying due to the harsh construction environment, which will affect the reliability of the measurement results. Therefore, it is crucial to utilize a bend-tolerant sensing fiber. Several special fibers came into existence, such as TA-OM4 fiber[13], trench-assisted or hole-assisted fiber[14-18] and microstructure photonic crystal fiber[19], which are based on the principle of introducing the trench-index profile around the core to suppress the optical signal loss caused by bending. These fibers have good compatibility with SMF and eliminate the complexity associated with fusion splicing. However, the bending resistances of these special fibers are not prominent, and the structures are generally complicated and the prices are also expensive. Therefore, they are less idea for practical SSHM applications when the ratio of performance to price is considered in larger scale distributed sensing.

In this paper, we combine a standard SMF as the input fiber with a 62.5 μm stepped index-multimode fiber (SI-MMF) as the sensing fiber in a frequency-shifted local heterodyne BOTDR system to achieve a single-ended distributed sensor with excellent bending resistance. This simple and inexpensive sensing structure has extremely prominent bending resistance and the minimum bend radius is 1.25 mm, which is superior to the sensing structures in Refs.[14—19]. We fuse a section of SMF at the near end of the MMF, which can be used as an exciter for the bend-tolerant fundamental mode and a filter for the bend-sensitive high-order modes in the MMF. The SMF is able to excite and select

* This work has been supported by the National Natural Science Foundation of China (Nos.61775057 and 51607066), the Natural Science Foundation of Hebei Province of China (Nos.F2019502112 and E2019502177), the Fundamental Research Funds for the Central Universities (Nos.2019MS086 and 2021MS071), and the S&T Program of Hebei (No.SZX2020034).

** E-mail: ncepufhj@163.com

the fundamental mode as much as possible, which reduces the effects of high-order modes coupling and improves the performance of the sensor. The principle and influencing factors of fiber bend loss are conducted, the bending resistances of different fibers are discussed, and a frequency-shifted local heterodyne BOTDR system is built to measure the bending resistances of different fibers. Finally, we measure and analyze the temperature sensing characteristics of the SMF alignment fusion to 62.5 μm SI-MMF.

In the long-distance sensing of a complete fiber, the optical loss is mainly divided into the inherent material loss and the bend loss. In the SSHM of SMF, the sharp deterioration of Brillouin signal caused by macrobend loss seriously affects the sensing distance and measurement reliability. The macrobend loss is divided into transition loss and pure bend loss[20,21], as shown in Fig.1. In the transition section between the straight and curved section, part of the power in the straight fiber excites the fundamental mode in the curved section, while the remaining power is coupled into the cladding, which results in a transition loss. The pure bend loss results from the continual loss of guiding at the outer portion of the evanescent field of the fundamental mode. This loss of guiding is due to the phase velocity of the outer part of the evanescent field equal to or even greater than the speed of light in the cladding.

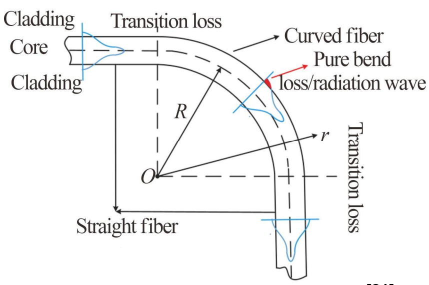


**Fig.1 Macrobend loss in SMF[21]**

When the fiber is straight, the cross-sectional internal field of the standard fiber is circularly symmetric. When the fiber is bent, the cross-sectional internal field is no longer circularly symmetric. As shown in Fig.2, the refractive index and effective refractive index of the SMF are tilted due to tension and extrusion. The refractive index increases on the outside of the curved fiber, and decreases on the inside. The tilted effective refractive index intersects with the refractive indexes of the core and cladding, dividing the curved fiber into a guided wave region, an evanescent wave region and a radiation wave region, which can be expressed by the transversal component of propagation vector[21].

$$k_{\mathrm{T}}(r)=\sqrt{\left[k_0 n(r)\right]^2-\beta^2(r)}=k_0\sqrt{n^2(r)-\beta^2(r)/k_0^2}=k_0\sqrt{n^2(r)-n_{\mathrm{eff}}^2(r)}, \tag{1}$$

where $\beta$ is propagation constant, $n(r)$ and $n_{\mathrm{eff}}(r)$ are respectively the refractive index and the effective refractive index of the fiber, and $k_0$ is propagation number of optical wave in vacuum. When $n(r)>\beta(r)/k_0$ and $n_2<n_{\mathrm{eff}}(r)<n_1$, this region is a guided wave region. When $n(r)<\beta(r)/k_0$, this region is an evanescent wave region. When $n(r)>\beta(r)/k_0$ and $n_{\mathrm{eff}}(r)<n_2$, this region is a radiation wave region, and only this region has optical loss. It follows that the smaller the bend radius of the fiber, the smaller the evanescent wave region, and the greater the optical power loss. Therefore, it is integral to expand the evanescent wave region in order to improve the bending resistance of fiber.

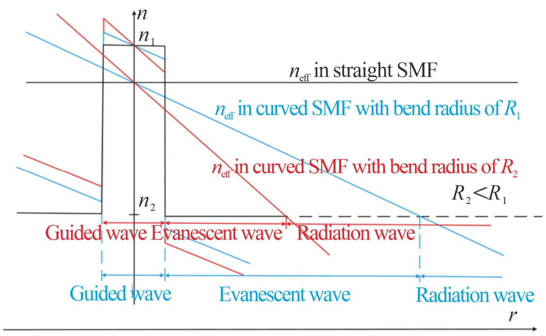


**Fig.2 Refractive indexes and wave regions distributions at different bends**

In order to expand the evanescent wave region of the fiber, the refractive index difference between the fundamental mode and the cladding can be appropriately increased. As shown in Fig.3, the larger the refractive index difference between the fundamental mode and the cladding, the larger the evanescent wave region of the fiber, the smaller the power loss, and the better the bending resistance.

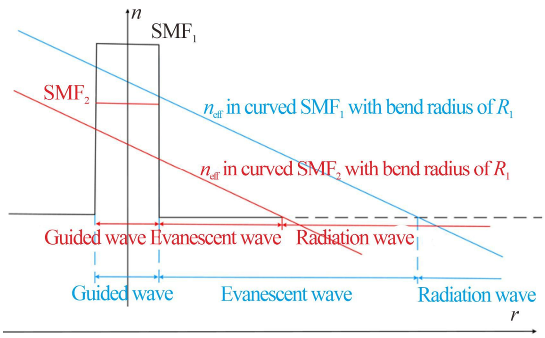


**Fig.3 Refractive indexes and wave regions distributions of different SMFs at the same bend**

In general, the relative refractive index difference of SMF is small, and is only about 0.3%—0.5%, which results in a small refractive index difference between the fundamental mode and the cladding. As a result, the evanescent wave region of SMF is small and its bending resistance is poor. Compared with SMF, the relative refractive index difference of MMF is much larger, and can be as large as about 1%—2%, which makes the refractive index difference between the fundamental mode and the cladding larger, so the fundamental mode of MMF has a better bend-tolerant capacity. However, since there are multiple modes in MMF and each mode has its own corresponding Brillouin gain spectrum (BGS), mode coupling and other interactions will occur between different modes, which will eventually lead to the broadening of BGS of the fiber and deterioration of the sensing performance. Therefore, it is vital to excite the fundamental mode as much as possible in MMF and filter out the high-order modes in the backscattering signal.

We utilized SMF alignment fusion to MMF to excite the fundamental mode in MMF. When the SMF is alignment fusion to MMF, only axially symmetric optical modes of the MMF are excited and the coupling coefficient between the SMF and the fundamental mode of the MMF is above 90%[22]. Therefore, the optical mode content of the sensing structure is mainly the fundamental mode. Fig.4 shows the electric fields of $LP_{01}$ and $LP_{11}$ modes in straight and curved MMF. It is obvious that the light field in the core has been transferred to the cladding.

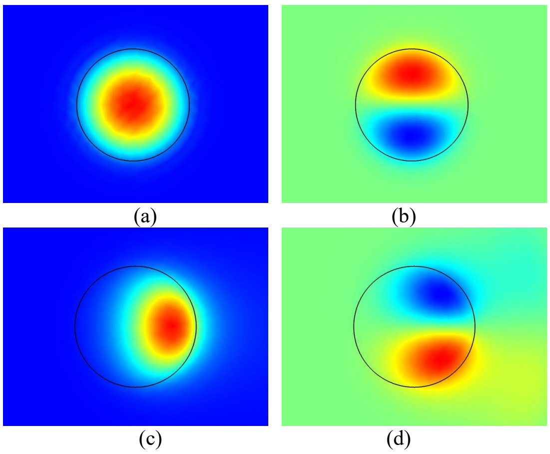


**Fig.4 Electric fields of (a) $LP_{01}$ in straight MMF, (b) $LP_{11}$ in straight MMF, (c) $LP_{01}$ in curved MMF, and (d) $LP_{11}$ in curved MMF**

The MMF is divided into SI-MMF and graded index-MMF (GI-MMF), usually with core diameters of 50 μm and 62.5 μm. The numerical aperture of 50 μm MMF is about 0.2, while for 62.5 μm MMF is about 0.275. Therefore, the 62.5 μm MMF is expected to have the best bending resistance. However, in the case of the same numerical aperture, the refractive index differences between the fundamental mode and the cladding of the two MMFs are different. The mode refractive indexes of SI-MMF and GI-MMF can be expressed as

$$n_{mn\text{SI-MMF}} = \frac{1}{k_0}\sqrt{k_0^2 n_0^2 - \left[\frac{\pi}{2}\left(m+2n+\frac{1}{2}\right)\right]^2 \Big/ a^2}, \quad (2)$$

$$n_{mn\text{GI-MMF}} = n_0\sqrt{1-\frac{2\sqrt{2\Delta}\left(m+n+1\right)}{k_0 n_0 a}}, \quad (3)$$

where $m$ denotes the number of whole standing waves distributed along the circumference of the field, $n$ denotes the number of half standing waves distributed along the radial direction of the field, $a$ is the fiber core radius of the MMF, $n_0$ is the refractive index of the MMF at $a$=0, and $\Delta$ is the relative refractive index difference of the MMF. The mode refractive indexes of the four MMFs are shown in Fig.5. $p$ is the mode group number, with $p=m+2n$ in SI-MMF and $p=m+n$ in GI-MMF. It is known that the 62.5 μm SI-MMF has the largest refractive index of the fundamental mode. As a result, compared with the fundamental mode in SMF and GI-MMF, the fundamental mode in SI-MMF has stronger bending resistance. The refractive indexes and wave regions distributions of SMF and two kinds of 62.5 μm MMFs at the same bend are shown in Fig.6.

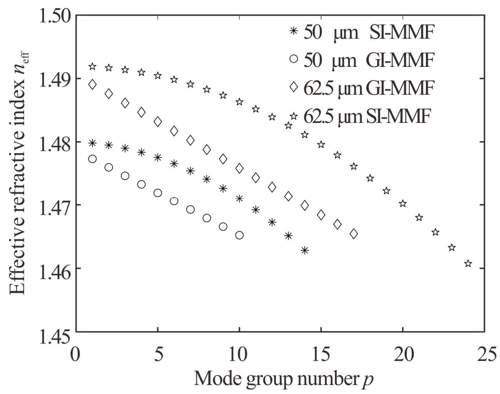


**Fig.5 Mode refractive indexes of the four MMFs**

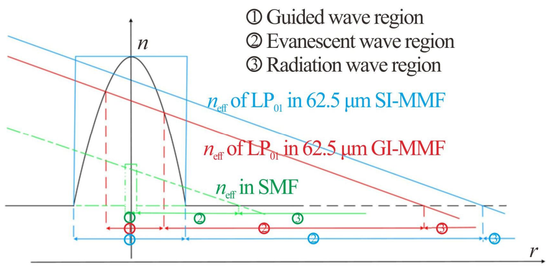


**Fig.6 Refractive indexes and wave regions distributions of SMF, 62.5 μm GI-MMF and 62.5 μm SI-MMF at the same bend**

A frequency-shifted local heterodyne BOTDR system is designed and constructed for evaluating the bending resistances of different sensing fibers, as shown in Fig.7. The output light of a laser diode (LD) with a central wavelength of 1 550.086 nm and a linewidth of 1.86 MHz is divided into pump light and local oscillator (LO) light by a 50: 50 polarization-maintaining coupler (PMC). A pulse generator (PG) is used to drive a high extinction ratio electro-optic modulator 1 (EOM1) to generate pump pulse. After being amplified by an erbium-doped fiber amplifier 1 (EDFA1), the pulse light enters a filter composed of an optical circulator 1 (OC1) and a fiber Bragg grating 1 (FBG1) with a central wavelength of 1 550.048 3 nm and a bandwidth of 0.251 4 nm to filter out the amplified spontaneous emission noise (ASEN). The pump pulse is adjusted to the appropriate power by a variable optical attenuator (VOA) and launched into the fiber under test (FUT), and the generated scattering light is amplified by EDFA3. The OC3 and FBG2 (central wavelength: 1 550.210 1 nm, bandwidth: 0.286 7 nm) are used to filter out ASEN and anti-Stokes signals. The light from lower arm is modulated into two sidebands, namely the continuous Stokes and anti-Stokes light, by EOM2 with an extinction ratio of greater than 40 dB that is operated in the suppressed carrier regime and is driven by a microwave generator (MG). A tunable optical filter (TOF) filters the carrier suppressed two sidebands signal after EDFA2 amplification, and only the lower sideband signal is retained. The polarization scrambler (PS) is used to randomly change the polarization state to reduce the signal fluctuation caused by polarization fading. After adjusting to the appropriate power by the VOAs, the beat signal of Brillouin scattering light and LO light are detected by a 1 GHz bandwidth photoelectric detector (PD) and collected by an electrical spectrum analyzer (ESA). The BGS is obtained by scanning the frequency offset of the scattering light and LO light. The Brillouin peak power trace is obtained by keeping the frequency of MG slightly larger than the *BFS* of the FUT, which provides a visual representation of the loss in the Brillouin signal.

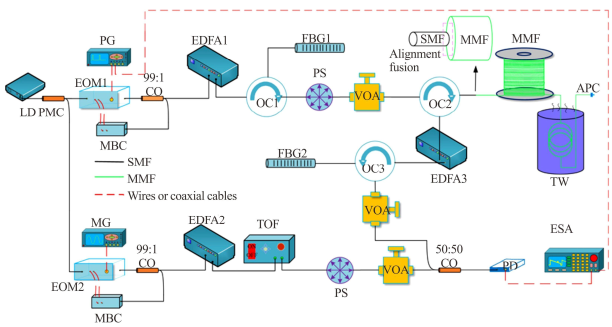


**Fig.7 Experimental setup**

In the experiment, the pulse width is set to 130 ns, which is limited by the maximum resolution bandwidth of the ESA of 8 MHz. It should be noted that all the devices except the FUT are single-mode devices in the experimental setup. In this experiment, SI-MMF and GI-MMF with the core diameter of 62.5 μm and the numerical aperture of 0.275 were alignment fusion to SMF to form the sensors. The peak power of pump pulse, scattering signal and LO light intensity are 1.5 W, 150 μW and 450 μW, respectively, which leads to a relatively high signal intensity. An interesting phenomenon has been noted in our experiment. Since a knot tied near the far end of the FUT cannot effectively reduce the Fresnel reflection signal from the fiber end, we fused a short length of the same fiber as the FUT with an angled polished connector (APC) to the end of FUT, and the Fresnel reflection signal of fiber end is almost eliminated totally, which is much different from the case using a standard SMF as sensing fiber and demonstrated the strong bend-tolerant capacity of our sensing structure in a simple and intuitive manner.

Using the system shown in Fig.7, we applied 10 turns with different bend radii at about 4.8 km of the sensing structure to simulate different degrees of bend in actual SSHM. After 10 measurements were averaged, the experimental results are shown in Fig.8. It can be seen that even if the 10 turns with bend radius of 1.25 mm were applied, the Brillouin signal of the SMF alignment fusion to 62.5 μm SI-MMF sensor has no obvious loss. As a comparison, the SMF alignment fusion to 62.5 μm GI-MMF sensor has a larger bend loss at a bend radius of 1.25 mm. The results indicate that the SMF alignment fusion to 62.5 μm SI-MMF has the best bend-tolerant capacity and the minimum bend radius is 1.25 mm, which is much better than the performance of Refs.[14—19]. The Brillouin signals of the sensing structures fluctuate slightly after bending, which indicates that there are a few high-order modes in the sensors. However, the fluctuation of the Brillouin signal is slight, and the bending resistance of the sensor is still prominent, indicating that the main optical mode in the sensing fiber is the fundamental mode. Moreover, due to the material resistance of the silica to macrobend, it is difficult to apply 10 turns with smaller bend radii. We have therefore determined that the minimum bend radius for this sensing structure is 1.25 mm.

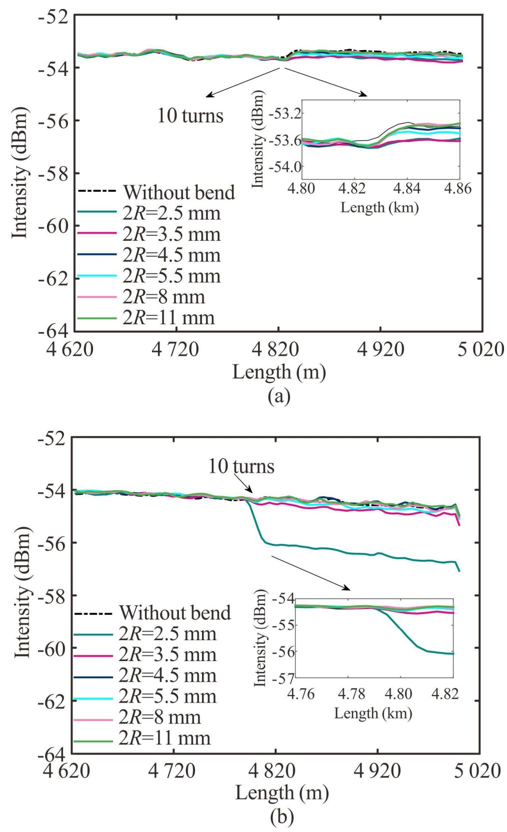


**Fig.8 Measured Brillouin signals with different bend radii for SMF alignment fusion to (a) 62.5 μm SI-MMF and (b) 62.5 μm GI-MMF**

In view of the good bending resistance of the SMF alignment fusion to 62.5 μm SI-MMF, we measured the temperature sensing characteristics of 5 km FUT. An approximated 120 m fiber near the far end of the FUT was placed in the thermostatic water (TW) with an accuracy of 0.01 °C, and a turn with bend radius of 1.25 mm was applied at 4.7 km and 4.95 km in the unheated section, respectively. The sensing fiber was warmed in steps of 10 °C from 35 °C to 75 °C, and each measurement and recording were performed after TW temperature reached the specified temperature for 20 min. The measurements were repeated three times and the results of the measurements are shown in Fig.9. Fig.9(a) shows the 3D BGS of the heating section at 75 °C. Fig.9(b) shows the *BFS* curves at different temperatures with a spatial resolution of 13 m, which corresponds to a pulse width of 130 ns. The calibrated temperature coefficient is 0.816 MHz/°C and is shown in Fig.9(c), which is slightly lower than that of SMF. The frequency shift fluctuation of the heating section is 0.56 MHz, so the temperature error of 0.69 °C can be obtained by using the calibrated temperature coefficient. Moreover, there is no significant change in Brillouin power and *BFS* at two bending points. These experimental results show that SMF alignment fusion to 62.5 μm SI-MMF has good performance as a sensing fiber in SSHM.

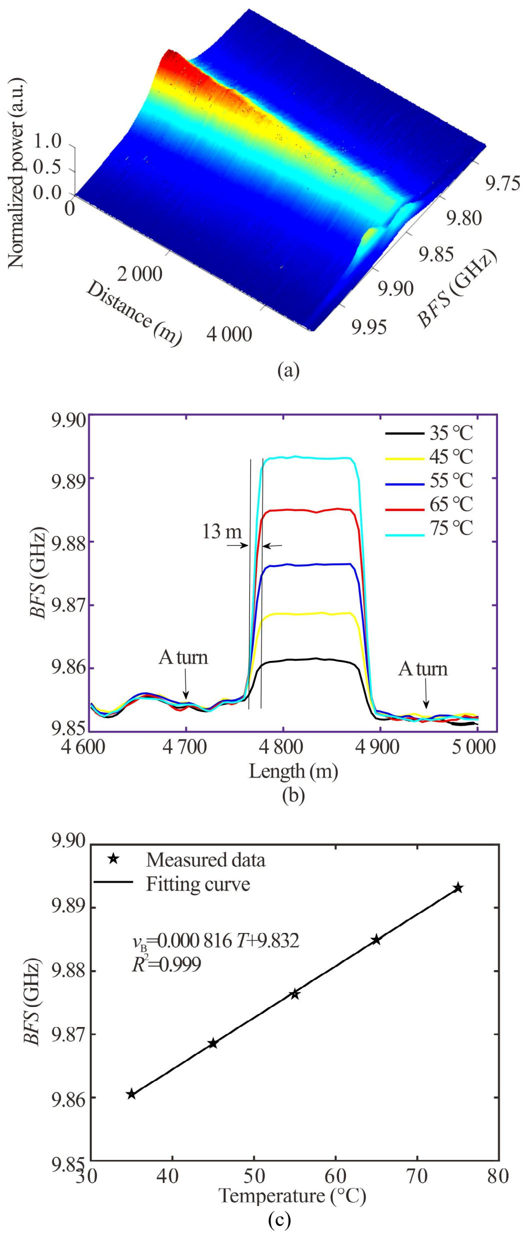


**Fig.9 Measured results: (a) 3D BGS with 75 °C; (b) *BFS* curves for different temperatures; (c) Linear relationship between *BFS* and temperature**

By the way, although there exist some high-order modes of vibration sensitivity in the sensing structure, we believe that our sensing structure has essentially the same vibration sensitivity as the SMF due to the dominant mode is fundamental mode and the presence of the mode filter of SMF at the beginning of the sensing structure. In addition, the BGS of the sensing structure based on MMF is wide, about 52 MHz, which is not conducive to the sensing accuracy of the sensor and is therefore an issue that needs to be addressed in our subsequent research.

In summary, we combine a standard SMF as the input fiber with a 62.5 μm SI-MMF as the sensing fiber in a frequency-shifted local heterodyne BOTDR system to realize bend-tolerant distributed sensing. The SMF is used as an exciter of the bend-tolerant fundamental mode in MMF and as a filter of the bend-sensitive high-order modes. We analyzed the influencing factors of fiber bend loss, compared the bending resistances of various fibers, and measured the minimum bend radius of the sensing structure as 1.25 mm. Moreover, we performed temperature measurements on this sensing structure and obtained a measurement error of 0.69 °C. Theoretical and experimental results show that the SMF alignment fusion to 62.5 μm SI-MMF has huge potential in the field of SSHM of large infrastructures.

## Statements and Declarations

The authors declare that there are no conflicts of interest related to this article.

## References

[1] BAO X Y, CHEN L. Recent progress in distributed fiber optic sensors[J]. Sensors, 2012, 12(7)：8601-8639.

[2] LIN R, ZHU Y F, TIAN L, et al. On-situ monitoring of sleet-thawing for OPGW based on long distance BOTDR[J]. Optoelectronics letters, 2021, 17(4)：226-230.

[3] GU K, SHI B, LIU C, et al. Investigation of land subsidence with the combination of distributed fiber optic sensing techniques and microstructure analysis of soils[J]. Engineering geology, 2018, 240：34-47.

[4] HU T, HOU G, LI Z. The field monitoring experiment of the roof strata movement in coal mining based on

DFOS[J]. Sensors, 2020, 20(5)：1-32.

[5] ZHANG X P. Distributed optical fiber sensing techniques[M]. Beijing：Science Press, 2013：18-25.

[6] WANG J J, LI Y Q, ZHANG L X. Performance enhancement for a self-heterodyne detection Brillouin optical time-domain reflectometer[J]. Optical engineering, 2020, 59(3)：034103.

[7] ZHAO J, YANG B, GUO F, et al. A new approach for quality monitoring based on multi-channel optical fiber[J]. Paper Asia, 2019, 2(3)：117-122.

[8] LI M, ZHANG Y, CHEN Z, et al. Investigation on the improvement of Brillouin optical time-domain reflectometer with Golay pulse codes in radiation environment[J]. Optical engineering, 2020, 59(4)：46102.

[9] LI Y Q, WANG L, ZHANG L, et al. Theoretical and experimental study on reducing coherent Rayleigh noise of Rayleigh scattering distributed optical fiber sensing system using PSK pulse coding[J]. Optical fiber technology, 2021, 64：102539.

[10] LI C L, LU Y G, ZHANG X P, et al. SNR enhancement in Brillouin optical time domain reflectometer using multi-wavelength coherent detection[J]. Electronics letters, 2012, 48(18)：1139-1141.

[11] YU Z H, ZHANG M Y, DAI H L, et al. Distributed optical fiber sensing with Brillouin optical time domain reflectometry based on differential pulse pair[J]. Optics and laser technology, 2018, 105：89-93.

[12] LI X J, LI Y Q, ZENG W X, et al. Performance improvement of a self-heterodyne detection BOTDR system employing broad-band laser[J]. Optoelectronics letters, 2018, 14(5)：325-330.

[13] ZHANG Z L, LU Y G, PAN Y H, et al. Trench-assisted multimode fiber used in Brillouin optical time domain sensors[J]. Optics express, 2019, 27(8)：11396-11405.

[14] ZHANG Y Q, LIAN Y D, WANG Y H, et al. Design and analysis of trench-assisted dual-mode multi-core fiber with large-mode-field-area[J]. Applied optics, 2021, 60(16)：4698-4705.

[15] JIA R J, LIAN Y D, WANG Y L, et al. Design and analysis of trench-assisted low-bending-loss large-mode-field-area multi-core fiber with an air hole[J]. Photonics, 2021, 8(7)：1-11.

[16] WANG G L, NING T G, PEI L, et al. A bending-resistant large mode area pixelated trench assisted segmented cladding fiber[J]. Optik, 2019：164024.

[17] XIE Y H, PEI L, ZHENG J J, et al. Impact analysis of a dense hole-assisted structure on crosstalk and bending loss in homogeneous few-mode multi-core fibers[J]. Optics express, 2020, 28(16)：23806-23819.

[18] SHE Y L, ZHOU D J, CHEN X Y, et al. Study on ultralow bending loss of bend-insensitive single mode optical fiber[J]. Optical fiber technology, 2019, 50：225-232.

[19] XU Z H, SHE Y L, ZHANG W T, et al. Ultralow bending-loss micro-structured fiber with large-mode-area[J]. Optik, 2022, 251：168440.

[20] XU P B, DONG Y K, ZHANG J W, et al. Bend-insensitive distributed sensing in singlemode-multi-mode-singlemode optical fiber structure by using Brillouin optical time-domain analysis[J]. Optics express, 2015, 23(17)：22714-22722.

[21] DONLAGIC D, CULSHAW B. Propagation of the fundamental mode in curved graded index multimode fiber and its application in sensor systems[J]. Journal of lightwave technology, 2000, 18(3)：334-342.

[22] MINARDO A, BERNINI R, ZENI L. Experimental and numerical study on stimulated Brillouin scattering in a graded-index multimode fiber[J]. Optics express, 2014, 22(14)：17480-17489.